High-Purity Multi-Mode Vortex Beam Generation With Full Complex-Amplitude-Controllable Metasurface

Quan Li, *Member, IEEE*, Chao Wu, *Member, IEEE*, Zhihui Zhang, Song Zhao, Bin Zhong, Song Li, Hongqiang Li, and Lijun Jin

***Abstract*— Vortex beam with inherent orbital angular momentum (OAM) is promising in high-capacity communication. On multimode vortex beam generation, metasurface has shown exceptional advantages of integration and miniaturization. For the current widely used phase-only methods on multimode vortex beam generation by metasurface, the purity of the OAM-mode spectrum is severely affected. A new method for generation of multimode vortex beam with high mode purity is proposed in this article by reconstructing the complete complex amplitude information on the meta-device aperture. A 20 dB suppression of the crosstalk modes is experimentally observed for the co-directional multimode vortex beam generation, which is much improved compared to the traditional phase-only scheme. In addition, the proposed scheme also provides the capability of generating high-purity multimode vortex beams with arbitrary preset propagation directions and power allocations. This study provides a platform for high-performance vortex beam communication by increasing the signal-to-noise ratio and enabling the multicasting scenarios with customized capacity requirements.**

***Index Terms*— High-purity, metasurface, multimode, vortex beam.**

I. Introduction

OPTICAL vortex beam with orbital angular momentum (OAM) [1] has shown great potential in a lot of fields, such as optical trapping [2], [3], [4], imaging [5], and communication [6], [7], [8], [9], [10]. Dual to the orthogonality of vortex beams with distinct OAMs, they provide additional degree of freedom to increase the available channels in communication [6], [7], [8], [10]. Vortex beam generation with specified OAM modes, propagation directions, and radiation powers is one of the crucial sections in OAM communication. In particular, the generation of multimode OAM beams from a single device under the shared illumination is essential in an OAM mode multicasting system [11], in which the message delivering direction and power of each multicasting OAM channel are usually arbitrary based on the specific scenarios. In the past two decades, various schemes have been proposed for vortex beam generation, including the spiral phase, computer-generated holograms [14], and circular antenna array [15], [16], [17]. Besides, metasurface with remarkable property of subwavelength electromagnetic field manipulation has also been utilized for vortex beam generation in recent years to overcome the limitation of flexibility in multimode integration and the miniaturization of devices of the traditional platforms [18], [19], [20], [21], [22], [23], [24], [25], [26], [27].

OAM-mode purity is one of the most important criterion of a high-quality vortex beam generator. For most of the current metasurfaces that generate single-mode vortex beam by constructing a spiral phase front, purity of the generated vortex beam is mostly impacted by several reasons, including the discretization of the device aperture to the meta-atom pixel array, the digitalization of the continuous spiral phase pattern to several certain phase levels, and the limited overall device aperture. As for multimode vortex beam generation, the complex amplitude distribution on the device aperture gets more complicated because of the superposition of multimode wavefronts. This will further increase the difficulty of wavefront recovering compared to the phase-only case for single-mode vortex beam generation. However, in most of the present works on multimode vortex beam generation, only phase information of the wavefront is considered, and the amplitude is simplified to be unity all over the device aperture [27], [28], [29]. Although some feedback algorithms have been proposed for complex phase pattern optimization so as to promote the OAM-mode purity [30], the overall design procedure is computationally intensive. Hence, there is still space in exploiting the underlying mechanism and techniques of high-purity multimode vortex beam generation meta-device.

According to the inherent correlation between the spatial field distribution and its OAM-mode spectrum, the lack of

Manuscript received 16 February 2022; revised 30 September 2022; accepted 3 October 2022. Date of publication 31 October 2022; date of current version 19 January 2023. This work was supported in part by the National Natural Science Foundation of China under Grant 11874286, Grant 11774057, Grant 61205041, and Grant U1966210; and in part by the Fundamental Research Funds for the Central Universities under Grant 20153638 and Grant 22120190222. *(Corresponding authors: Chao Wu; Hongqiang Li.)*

Quan Li is with the College of Electronic and Information Engineering, the School of Physics Science and Engineering, and the Shanghai Key Laboratory of Special Artificial Microstructure Materials and Technology, Tongji University, Shanghai 200092, China (e-mail: 1210583@tongji.edu.cn).

Chao Wu and Hongqiang Li are with the College of Electronic and Information Engineering, the School of Physics Science and Engineering, and the Shanghai Key Laboratory of Special Artificial Microstructure Materials and Technology, Tongji University, Shanghai 200092, China, and also with the Innovation Center, Institute of Dongguan-Tongji University, Dongguan, Guangdong 523808, China (e-mail: chaowu@tongji.edu.cn; hqlee@tongji.edu.cn).

Zhihui Zhang and Song Zhao are with the School of Physics Science and Engineering and the Shanghai Key Laboratory of Special Artificial Microstructure Materials and Technology, Tongji University, Shanghai 200092, China (e-mail: zhaosong@tongji.edu.cn; 1830984@tongji.edu.cn).

Bin Zhong is with the Innovation Center, Institute of Dongguan-Tongji University, Dongguan, Guangdong 523808, China (e-mail: zhongb@idtu.cn).

Song Li is with the State Key Laboratory of Advanced Fiber Composite, Beijing 102101, China (e-mail: lisong1996@126.com).

Lijun Jin is with the College of Electronic and Information Engineering, Tongji University, Shanghai 200092, China (e-mail: jinlj@tongji.edu.cn).

This article has supplementary material provided by the authors and color versions of one or more figures available at https://doi.org/10.1109/TAP.2022.3217192.

Digital Object Identifier 10.1109/TAP.2022.3217192

amplitude information leads to the distortion of OAM-mode spectrum, and hence, the purity of the desired dominant modes will drop and the crosstalk modes increase as noises. Obviously, both the amplitude and phase information are needed to precisely construct the multimode vortex beams. In addition, considering the practical applications, it is also necessary to generate a series of vortex beams that propagate along different directions with certain OAMs and power allocations, that is, a specific distribution in OAM state space. To this end, the reconstruction of both phase and amplitude information of multimode vortex beam wavefront is also demanded.

In this article, we propose a method for multimode vortex beam generation based on complete reconstruction of the desired complex wavefront. The high mode purity is quantitatively analyzed and verified through both numerical calculation and experimental measurement. As examples, two multimode vortex beam generators operating in microwave regime are designed and characterized: the first one generates three-mode vortex beams that propagate along the same direction and the second one generates three vortex beams of different OAM modes that propagate toward distinct directions with different powers. As a comparison, we also investigate their traditional counterparts, for which only phase distributions are considered, while the amplitudes remain uniform across the corresponding device apertures. Both the calculations and measurements show enhanced mode purity by introducing full complex amplitude modulation, compared with the traditional phase-only scheme. A 20 dB suppression of the crosstalk mode is experimentally observed for the co-directional propagation case and about 15 dB for the multidirectional propagation case.

II. Concept and Meta-Atom Design

The crux of the proposed high-purity multimode vortex beam generation scheme is imparting arbitrary independent phase and amplitude distributions onto electromagnetic wavefront, which is a highly desirable goal in metasurface research. By exploiting combination of degrees of freedom such as position, orientation, and size, various strategies have been proposed to obtain full-range complex amplitude modulation [31], [32], [33], [34], [35], [36]. A novel approach is to use cascaded bilayer anisotropic structures as meta-atom [37], in which full-range complex amplitude modulation for spin waves is achieved by tuning the orientations of two layers. The amplitude of transmitted circular-polarization conversion component is determined by the difference between two orientation angles, whereas the phase is determined by the summation of them. For simplifying the multimode vortex beam generator design, we adopt this complex amplitude modulation strategy because it avoids lots of time-consuming geometric parameters searching in a meta-atom design. It is noteworthy that other complex amplitude modulation methods can also be used to implement the proposed multimode vortex beam generation scheme, and the generated vortex beams can have polarization states other than circular-polarized states.

A schematic of high-purity multimode vortex beam generation based on full complex-amplitude-controllable metasurface is shown in Fig. 1. Under normal illumination of right-handed circularly polarized (RCP) waves, the transmitted left-handed circularly polarized (LCP) waves get converted into several vortex beams with different topological charges. Due to the full and arbitrary complex amplitude modulation feature of the proposed metasurface, both the amplitude and phase information at each position of the wavefront are simultaneously and directly reconstructed for multimode vortex beam generation. Therefore, the crosstalk modes are extremely suppressed in contrast to the traditional phase-only generation scheme. In addition to the high mode purity, the proposed scheme of applying complex amplitude modulation also provides a practical approach for generating multimode vortex beams that propagate along different directions with customized power allocation.

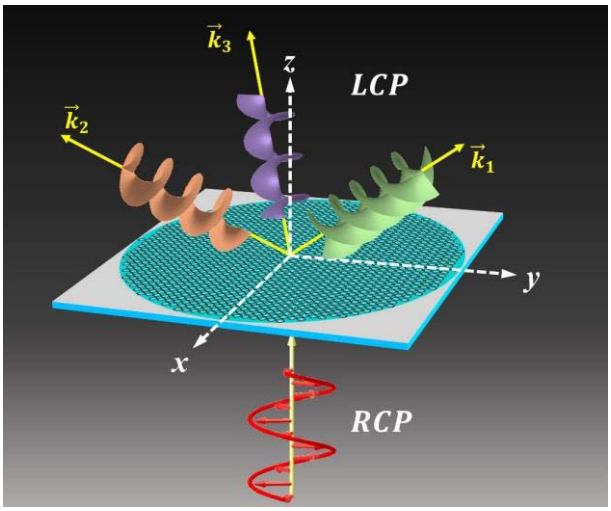

Fig. 1. Schematic of high-purity multimode vortex beam generation.

As shown in Fig. 2(a), a bilayer ring-shielded-bowtie structure is adopted as meta-atom, which is the basic building block of the proposed vortex beam generator. Two planar metallic resonating structures with the same physical dimensions except for the orientation angles are manufactured on the two sides of a dielectric substrate F4B ($\varepsilon_r = 2.65$ and $\tan\delta = 0.0017$). The orientation angles of the two structures are defined as the angle between the symmetry axis of each layer [blue dashed-dotted lines in Fig. 2(a)] and the x-axis, and marked as α_1 and α_2. The geometric parameters are the outer radius of the circular ring $r_1 = 3.15$ mm, the inner radius $r_2 = 0.65$ mm, the width of the circular ring $w_1 = 0.3$ mm, the gap width between the circular ring and the bowtie structure $w_2 = 0.2$ mm, the open angle of the bowtie structure $\gamma = 60°$, and the lattice constant $p = 7$ mm. The transmission spectra in circular basis with both orientation angles being 0° are calculated using the commercial software *Eastwave* [38] and shown in Fig. 2(b). For the meta-atom design, periodic boundary conditions are applied at both the x and y boundaries and perfectly matched layers at the z boundaries. Circularly polarized incident plane wave is set to be along the z-direction. It can be seen that the circular-polarization conversion reaches the maximum efficiency of 93.9% at 10.15 GHz. As inspired by [37], by tuning the two orientation angles, an arbitrary combination of phase from 0° to 360° and amplitude from

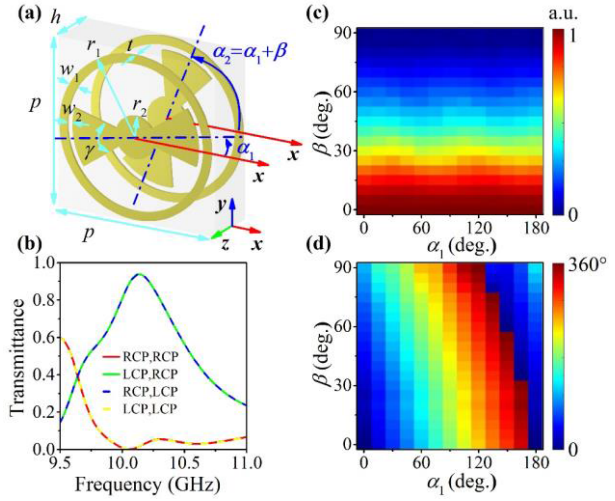

Fig. 2. (a) Schematic of the meta-atom structure; (b) calculated transmittance spectra in circular basis for meta-atom with orientation angles α_1 and α_2 both being zero, where the first and the second subscripts in the legend refer to the polarization state of the transmitted and incident waves, respectively; (c) normalized amplitude; and (d) phase shift of RCP-to-LCP conversion component compared to the $(\alpha_1, \alpha_2) = (0°, 0°)$ orientated meta-atom as functions of α_1 and β at 10.15 GHz.

zero to the maximum efficiency can be achieved for circular-polarization conversion components.

The transmission spectra of RCP-to-LCP conversion components are further investigated for meta-atoms with other orientation angles. The normalized amplitude and phase are shown in Fig. 2(c) and (d), respectively. Obviously, the normalized amplitude is determined by the orientation angle difference $\beta = \alpha_2 - \alpha_1$ and varies from 0 to 1 as β decreases from 90° to 0°. On the other hand, the phase can be modulated in the range of [0°, 360°) by further tuning the orientation angle α_1. Note that we do not strictly follow the two cascaded quarter-wave plate design in [37], and the relationship between orientation angles and complex amplitude is also altered. However, based on the same mechanism, full-range complex amplitude modulation is also achieved with the more compact bilayer meta-atom. Then, arbitrary phase and amplitude control over electromagnetic wavefront can be implemented with the proposed meta-atom, which may find various advanced applications, including multimode vortex beam generation.

III. Meta-Device Design

We now describe the method of high-purity multimode vortex beam generation by employing the proposed meta-atom. For simultaneous generation of N vortex beams with respective topological charges l_n and amplitude E_n, the complex amplitude distribution in the xoy plane can be described as

$$A(x, y) = \sum_{n=1}^{N} E_n \exp^{il_n\varphi} \exp^{i(k_0 x \sin\theta_n \cos\varphi_n + k_0 y \sin\theta_n \sin\varphi_n)} \quad (1)$$

where (θ_n, φ_n) with $n = 1, 2, 3, \ldots, N$ are the elevation and azimuth angles that represent the propagation directions of the corresponding vortex beams, respectively. We first demonstrate a case to generate three vortex beams with the same propagation direction (z-axis) and power. The topological charges

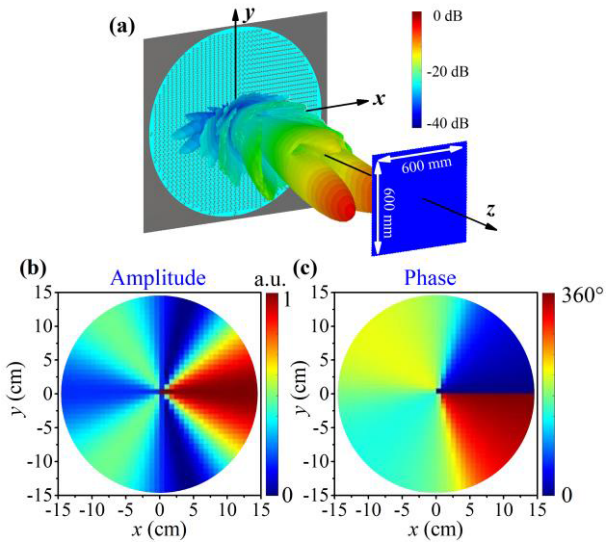

Fig. 3. (a) Schematic of the three-mode vortex beam generator with complex amplitude modulation, (b) corresponding normalized amplitude, and (c) phase distribution on the device aperture.

are set to be $(l_1, l_2, l_3) = (+1, +2, -1)$. The vortex beam generator is schematically shown in Fig. 3(a). Considering the circular symmetry of vortex beams, the device composed of 1257 meta-atoms in total is designed to cover a circular region, that is, a round area with a radius of $20 \times p$ intercepted at the center of a square array. The rest area of the sample is covered by continuous copper film. The corresponding normalized electric field (E-field) amplitude and phase distribution in the xoy plane are derived from (1) and shown in Fig. 3(b) and (c). Then, the distributions of the meta-atom orientation angles are determined according to the relationship shown in Fig. 2(b) and (c). Namely, the orientation angle difference β is first derived through interpolation based on the amplitude values shown in Fig. 2(b), and then, the orientation angle of the first layer α_1 is also derived through interpolation based on the phase values shown in Fig. 2(c). For comparison, we also design a traditional phase-only multimode vortex beam generator with the proposed meta-atom. Though having the same size as our complex amplitude-modulated devices, only the phase distribution shown in Fig. 3(c) is reconstructed, with the amplitude staying uniform across the device aperture. In terms of the meta-atom, the parameter α_1 is still determined in the aforementioned manner, while the orientation difference β is set to 0° everywhere.

Both the complex amplitude-modulated and phase-only devices are fabricated by the standard printed-circuit-board technique on F4B substrates (Taconic TLT-6). The photographs of sample and experiment setup are shown in Fig. 4. The measurements are performed in an anechoic chamber with Keysight PNA-X 5242A Network Analyzer. An RCP horn antenna is used to generate normal incident wave. With a small helix antenna that is mounted on a translation stage as probe, the transmitted LCP E-field component is measured in steps of 1 mm within a 600×600 mm area on the plane 700 mm above the device surface. Fig. 5 shows the calculated and experimentally measured LCP E-field distributions together with the corresponding OAM-mode spectra of the two

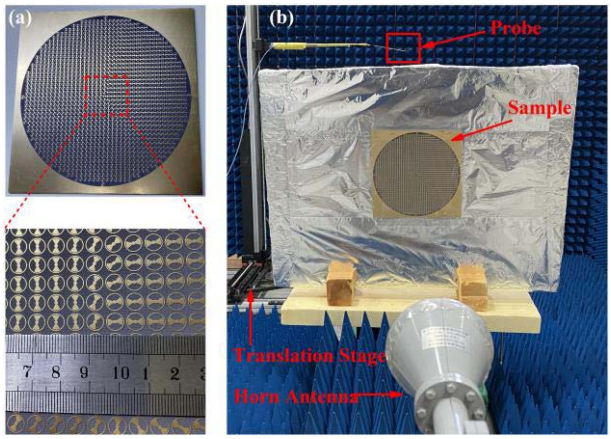

Fig. 4. (a) Photograph of the manufactured sample. The enlarged view in the inset shows the orientation variation of meta-atoms in the selected region. (b) Experiment setup of field sampling measurement.

meta-devices. Fig. 5(a)–(f) shows the results of the device with complex amplitude modulation and Fig. 5(g)–(i) corresponds to the phase-only one. The field calculation of all the devices in this work is also implemented with the commercial software *Eastwave*. As for the meta-devices design through full-wave simulation, perfectly matched layers with vacuum spacer are applied at all six boundaries. RCP plane waves along the z-direction are used to excite the structures. Note that the amplitude distributions in Fig. 5 are all normalized to their respective global maxima. Clearly, the measured amplitude and phase distributions agree very well with the calculated ones, except for some disturbance that is mainly caused by the weak scattering from the measurement environment.

In order to analyze the mode purity of generated multimode vortex beam, the OAM-mode spectra are extracted from both the calculated and measured E-field distributions. By sampling the fields within a circular region, the powers of different OAM modes are obtained by [39]

$$P_l = \frac{1}{2\pi}\int_0^{\infty}\left|\int_0^{2\pi} u(x,y,z)\cdot e^{-il\varphi}d\varphi\right|^2 r\,dr \tag{2}$$

and then normalized by the global maximum power in the spectra. Specifically, in accordance with the circular symmetry of the vortex beam, a circular integral region is adopted. The radius $R = 200$ mm (white circle in Fig. 5) is chosen to include most of the power of the three dominant modes. Only spectra for OAM modes of $l \in [-5, +5]$ are presented because the power of modes with $|l| > 5$ is too weak to impact the conclusion.

As can be found in Fig. 5(c), the calculated level of the crosstalk modes is around -40 dB for the device with complex amplitude modulation, and the calculated OAM-mode spectrum components of $l = +1, +2$, and -1 are nearly equal, which is consistent with our design. It is worth noting that the power of the spectrum component of $l = +2$ is a little smaller (about 1.13 dB) than those of modes $l = \pm 1$. This mainly originates from the divergence nature of vortex beams and the divergence angle becomes larger as the abstract value of mode number $|l|$ increases. Consequently, less energy is collected within a circular sampling region of fixed radius for vortex beams with a relatively larger mode number. The detailed analysis about this point can be found in the Supplementary Material. In contrast, as shown in Fig. 5(i), powers of the crosstalk modes are much bigger for the phase-only device, which reaches about -10 dB. In addition, the maximum power deviations of the dominant modes are also bigger (about 1.7 dB). In particular, powers of modes $l = +1$ and $l = -1$ are not equal to each other, though they have the same divergence angle. These phenomena are all mainly caused by the absence of amplitude information when reconstructing the wavefront of multimode vortex beams.

The measured mode spectra for complex amplitude modulation and phase-only devices are shown in Fig. 5(f) and (l), respectively. Clearly, the measured results are basically coincident with the calculated ones. Though crosstalk modes are stronger due to the inevitable factors such as antenna misalignment, fabrication errors, and environmental scattering, the dominant OAM modes of $l = +1, +2$, and -1 of the complex amplitude modulation device are still bigger than the other crosstalk OAM modes by about 20 dB. For the phase-only device, though the dominant modes can also be distinguished but are only about 10 dB bigger than the crosstalk modes, the calculated and measured results show clearly that, compared to the phase-only case, the mode purity of the generated multimode vortex beams gets significantly improved when the complex amplitude information of wavefront is reconstructed. More precisely, the spectrum of the dominant modes is closer to the designed values and the crosstalk modes are reduced by more than 10 dB. This is crucial in OAM multiplexing data transmission to increase the channel capacity and energy efficiency due to the signal-to-noise ratio optimization.

Besides, the device efficiencies are compared between the complex amplitude case and the phase-only case. Since both devices are designed to generate OAM beams of order $l = +1, +2$, and -1, the effective transmission power is the summation of the powers of these three modes. A reasonable and straightforward efficiency comparison can be implemented by calculating the ratio of effective transmission powers of the two cases

$$\sum_{l=-1,1,2} P_l^{complex\ \ amplitude} \Big/ \sum_{l=-1,1,2} P_l^{phase\ \ only} \tag{3}$$

which is 77.2% and 81.8% for simulated and measured results, respectively. In addition, to show the efficiency of the proposed devices more comprehensively, another two indices are also calculated. One of them is the polarization conversion efficiency, which is the ratio of the power carried by cross-polarized OAM modes to the total incident power. The other is the effective power ratio, which is the ratio of the power carried by three designed OAM modes to the total cross-polarized transmitted wave. These two definitions have been adopted in many previous works [40], [41], [42], [43], and the calculated and measured results for our devices are obtained by the following equations and shown in Table I.

The polarization conversion ratio is calculated by

$$\eta_1 = \frac{\Sigma_l P_l}{P_i} \tag{4}$$

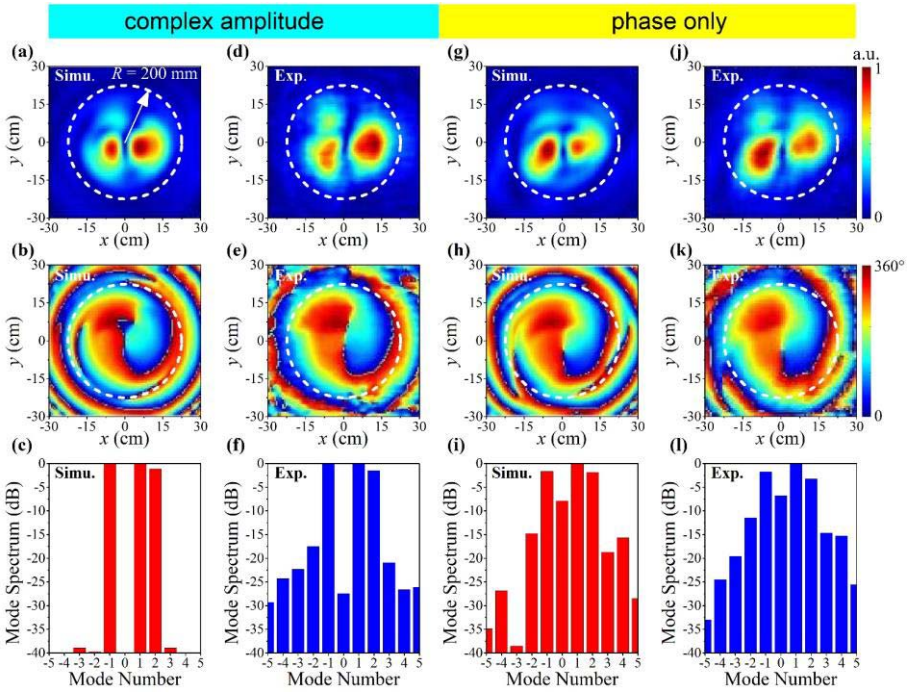

Fig. 5. Calculated results of the normalized LCP E-field distribution on the specified sampling plane (a) and (b) distracted OAM-mode spectrum and (c) corresponding measurement results of (d)–(f) device with complex amplitude wavefront modulation. Calculated results of the normalized E-field distribution on the specified sampling plane, (g) and (h) distracted OAM-mode spectrum and (i) corresponding measurement results of (j)–(l) control group device with phase-only wavefront modulation. The amplitude distributions are all normalized to their respective global maxima.

TABLE I

CALCULATED AND MEASURED POLARIZATION CONVERSION EFFICIENCIES AND EFFECTIVE POWER RATIOS FOR CO-DIRECTIONAL THREE OAM MODES GENERATION BASED ON PHASE ONLY AND COMPLEX AMPLITUDE MODULATION

	Phase Only Simu.	Phase Only Exp.	Complex Amplitude Simu.	Complex Amplitude Exp.
η_1	63.6%	56.2%	44.5%	39.91%
η_2	90.61%	85.46%	99.98%	98.43%

and the effective power ratio is calculated by

$$\eta_2 = \frac{\Sigma_{l=-1,+1,+2} P_l}{P_{t,\mathrm{lcp}}} \tag{5}$$

where P_i refers to the total incident power and $P_{t,\mathrm{lcp}}$ is the total transmitted power of the cross-polarized (LCP) component.

Obviously, obtaining high mode purity with complex amplitude modulation approaches does accompany with certain decrease of the device efficiency. However, the effective power ratio of complex amplitude modulation case is higher than that of the phase-only one. Then, the effective transmission power of complex amplitude case is rather close to the phase-only one.

Based on the proposed method, by applying complex amplitude modulation, it is also promising to construct multimode vortex beams that propagate along arbitrary distinct directions with different powers, which is significant for multicasting communication scenarios. Consider generation of three vortex beams with the OAM modes of $(l_1, l_2, l_3) = (+1, +2, -1)$, the power ratio of $P_1{:}P_2{:}P_3{:} = 3{:}2{:}1$, and the propagation direction of $(\theta_1, \theta_2, \theta_3) = (10°, 10°, 20°)$ and $(\varphi_1, \varphi_2, \varphi_3) = (0°, 0°, 90°)$; the complex amplitude distribution in the xoy plane can also be obtained by (1). Following the same procedure, the corresponding device is designed in the same size, and the normalized amplitude and phase distribution over the meta-device aperture are shown in Fig. 6(b) and (c), respectively.

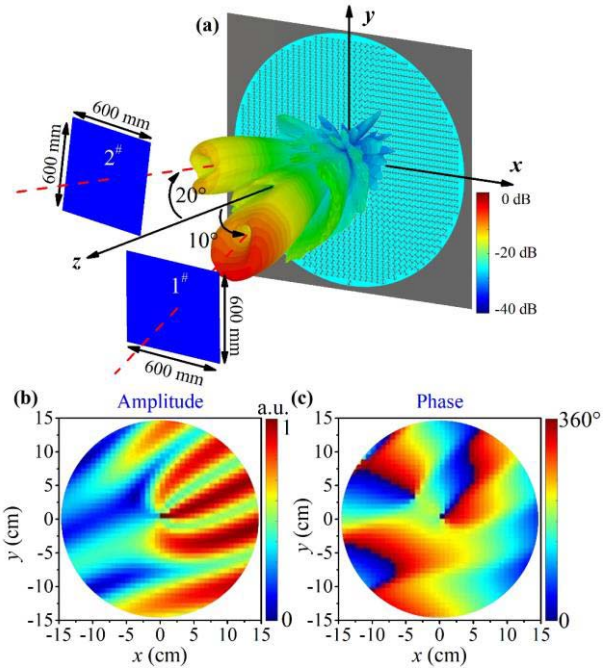

Fig. 6. (a) Schematic of the device for generation three-mode vortex beam with specified topological charges, propagating directions, (b) power allocations and the corresponding normalized amplitude, and (c) phase distribution pattern on the device aperture.

The far-field pattern of the designed metasurface is shown in Fig. 6(a). Two lobes are clearly identified in which the lobe

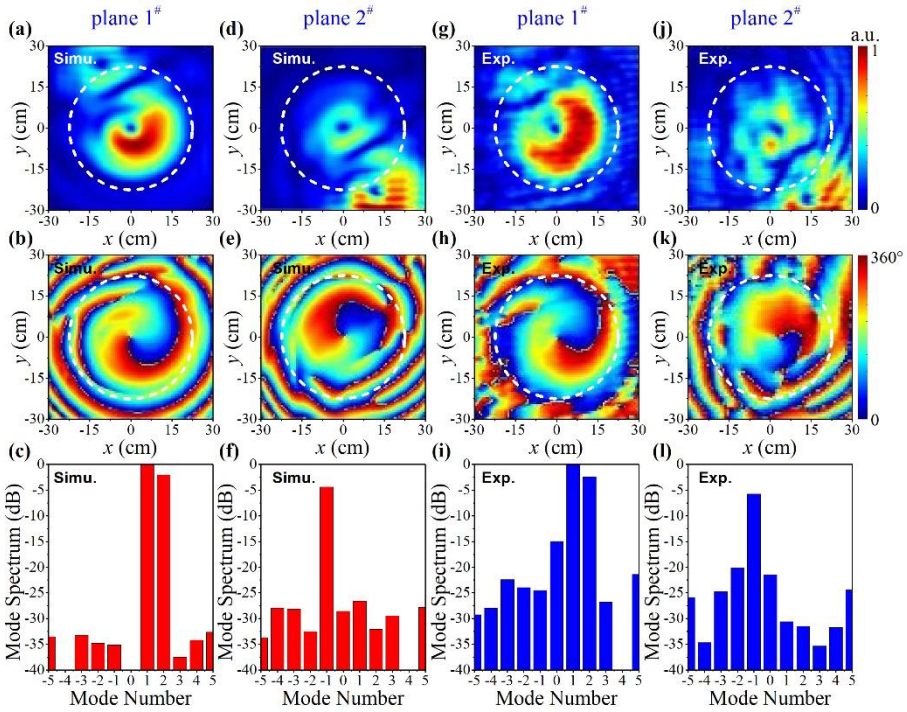

Fig. 7. Calculated and measured results of the device (complex amplitude case) for generating three-mode vortex beam with specified topological charges, propagating directions and power allocations. Calculated results of the normalized LCP E-field distribution and the distracted OAM-mode spectrum on (a)–(c) specified sampling plane 1# and (d)–(f) sampling plane 2#. Measured results of the normalized E-field distribution and the distracted OAM-mode spectrum on (g)–(i) specified sampling plane 1# and (j)–(l) sampling plane 2#. The amplitude distributions are normalized to their respective global maxima.

with axis lying in the yoz plane corresponds to the single vortex mode of $l = -1$ with relatively lower power, while the other lobe with axis lying in the xoz plane represents the mixed vortex modes of $l = +1$ and $l = +2$ with relatively higher powers. To observe the magnitude and phase distribution of the lobes, two transection sampling planes with size of 600 × 600 mm are adopted 700 mm away from the metasurface aperture center.

Fig. 7 shows the calculated and measured results on the predefined sampling planes of the metadevice with complex amplitude modulation. The amplitude distributions are also normalized to their respective global maxima. The OAM-mode spectra are then extracted from the LCP E-field sampling values and normalized to the corresponding global maximum. For the calculation results in Fig. 7(e) and (f), the power ratio of the three dominant modes is $P_1{:}P_2{:}P_3{:} = 0{:}-2.04{:}-4.38$ dB, which slightly deviates from the desired value of $P_1{:}P_2{:}P_3{:} = 0{:}-1.76{:}-4.77$ dB or $P_1{:}P_2{:}P_3{:} = 3{:}2{:}1$ in a linear form. Notice that the integral region for OAM-mode spectrum calculation here is also within a circle of radius $R = 200$ mm. Although a fraction of E-field of the neighboring lobe is collected in both of the two sampling planes, the power of the corresponding dominant mode is hardly impacted and the good agreement of the extracted dominant mode spectrum with the theoretical values also verifies this point, while for the crosstalk modes, considering the interference from the neighboring lobe, the calculated results still show a low level of about −30 dB.

The E-field distributions are also experimentally measured in microwave chamber, followed by the OAM-mode spectrum analysis. As shown in Fig. 7(g)–(l), the E-field amplitude and phase distributions agree well with the calculated ones in both planes 1# and 2#, in which the most remarkable is the singularity point in each plane that is almost in the center, indicating that the two lobes are propagating in the designed directions. The measured power ratio of the three dominant OAM modes is $P_1{:}P_2{:}P_3{:} = 0{:}-2.44{:}-5.78$ dB, as shown in Fig. 7(i) and (l), which slightly deviates from the calculated one because of the aforementioned inevitable measurement errors. A phase-only device is also constructed and characterized for comparison, for which only the phase information in Fig. 6(b) is reconstructed and the amplitude is uniform across the device aperture. The results can be found in Fig. 8.

As clearly indicated in Fig. 8, both the calculated and measured results show much higher power levels of the crosstalk modes for phase-only devices, compared to those shown in Fig. 7. In addition, the calculated power ratio of the three dominant modes is $P_1{:}P_2{:}P_3{:} = 0{:}-3.95{:}-5.3$ dB, which obviously deviates from the designed value of $P_1{:}P_2{:}P_3{:} = 0{:}-1.76{:}-4.77$ dB. All the calculated and measured results verified the purity improvement of the generated multimode multidirectional vortex beams, indicating the feasibility of the proposed method in this article.

Efficiency analysis is also implemented for multidirection trimode devices. Based on the calculation and experimental results that are extracted from the sampling planes consistent with the abovementioned mode purity analysis, the ratios of effective transmission power in the two cases are also calculated by (3), which are 80.12% and 78.28% for simulated and measured results, respectively. The quite close effective transmission powers of the complex amplitude case and the phase-only case are also observed.

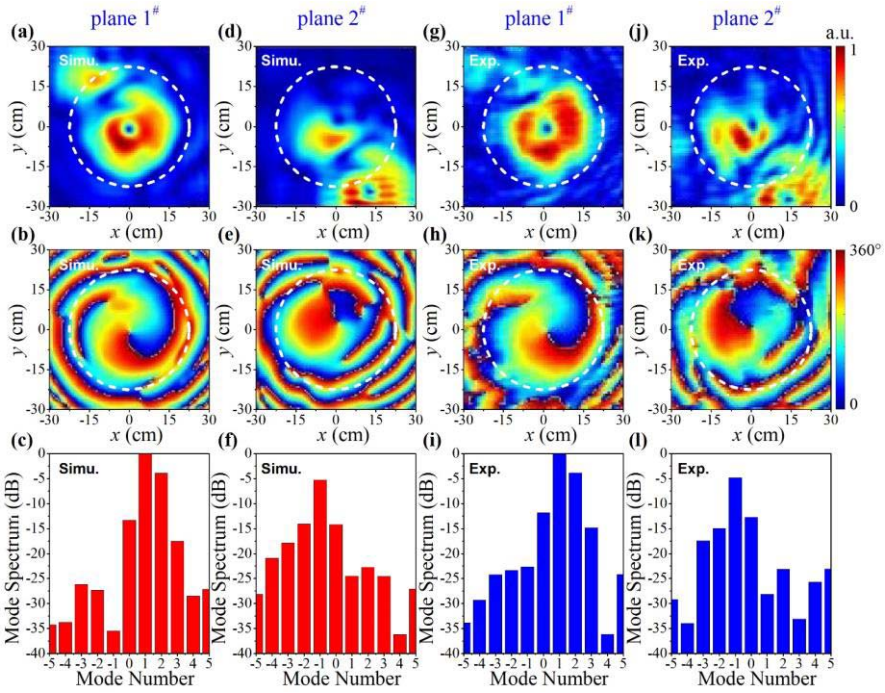

Fig. 8. Calculated and measured results of the device (phase-only case) for generating three-mode vortex beam with specified topological charges, propagating directions and power allocations. Calculated results of the normalized LCP E-field distribution and the distracted OAM-mode spectrum on (a)–(c) specified sampling plane 1# and (d)–(f) sampling plane 2#. Measured results of the normalized E-field distribution and the distracted OAM-mode spectrum on (g)–(i) specified sampling plane 1# and (j)–(l) sampling plane 2#. The amplitude distributions are normalized to their respective global maxima.

TABLE II

CALCULATED AND MEASURED POLARIZATION CONVERSION EFFICIENCIES AND EFFECTIVE POWER RATIOS FOR MULTIDIRECTIONAL THREE OAM MODES GENERATION BASED ON PHASE ONLY AND COMPLEX AMPLITUDE MODULATION

	Phase Only Simu.	Phase Only Exp.	Complex Amplitude Simu.	Complex Amplitude Exp.
η_1	65.64%	58.28%	47.62%	40.33%
η_2	89.92%	87.96%	99.3%	99.5%

TABLE III

CALCULATED FRACTIONS OF POWER INCIDENT FROM THE FEED HORN AND REFLECTED FROM THE METASURFACE FOR BOTH CO-DIRECTIONAL AND MULTIDIRECTIONAL THREE OAM MODES GENERATION BASED ON PHASE ONLY AND COMPLEX AMPLITUDE MODULATION

	Complex Amplitude (Simulation).	Phase Only (Simulation).
Co-directional	47.6%	31.6%
Multi-directional	43.3%	29.7%

TABLE IV

CALCULATED RATIOS OF COMMUNICATION DISTANCE AND THE FAR-FIELD LIMIT $2D^2/\lambda$ FOR [6], [8], [44], AND FOR OUR WORK

Ref.	D	λ	$2D^2/\lambda$	*distance*	*ratio*
[6]	30 cm	10.7 mm	16.8 m	2.5 m	0.15
[8]	7.68 mm	1550 nm	76 m	Not indicated. Judged to be meter level	0.013~0.13
[44]	11 m	532 nm	$4.55*10^5$ km	143 km	0.00031
This work	400 mm	29.6 mm	10.8 m	0.7 m	0.065

Similarly, we also investigate the polarization conversion efficiencies and the effective power ratios of multidirectional propagation cases. The results are shown in Table II.

In addition, though the efficiency of complex amplitude case decreases a little bit, the mode purity and power allocation accuracy between different modes are significantly improved, and the overall performance of complex amplitude case still has obvious advantages for high-precision anti-interference communication and other applications.

To reveal the performance of the proposed devices more comprehensively, we further calculate the fractions of power incident from the feed horn and reflected from the metasurfaces. The calculated results under RCP incidence are shown in Table III.

To avoid misunderstanding, we need to point out that there is also a small fraction of energy in the form of co-polarized transmitted waves. However, the power fraction is rather small (less than 8% for all cases).

Last but not least, we want to point out that most works contributing to the OAM multiplexing technique, including our findings, are mainly operating in the near field, due to the severe power decay of the vortex mode in long-distance transmission for a fixed receiving aperture. Several recent works [6], [8], [44] are taken as example, and the ratios between the communication distances and the far-field limit $2D^2/\lambda$ are calculated. The results are shown in Table IV, where D is the size of the larger aperture of either the receiving or the transmitting antenna in the corresponding reference and *distance* represents the actual communication distance in the corresponding reference or, in our work, the distance between the meta-device and the sampling plane. Then, the *ratios* of distances and $2D^2/\lambda$ are calculated and shown in the last column.

The results clearly indicate that the mentioned references as well as our findings are all operating in the near field. However, we want to point out that despite the well-known near-field limitation, vortex beam communication is still a promising alternative approach to improve spectrum efficiency, as has been verified in specific near-field application scenarios in the references. The proposed scheme for high mode purity OAM generation may find applications in various fields beyond near-field communication.

IV. Conclusion

In summary, by reconstructing both the amplitude and phase information in the wavefront, we design, fabricate, and experimentally verify a meta-device for multimode vortex beam generation that exhibits high purity of the dominant modes in the OAM-mode spectrum. In addition, the significant suppression of the crosstalk modes by more than 20 dB is observed for the co-directional propagation case and about 15 dB for the multidirectional propagation case, which are both much improved compared to their phase-only counterparts. Though the proof-of-principle devices are designed in radio frequency, it is convenient to be generalized to other regimes, including terahertz and optics by constructing similar bilayer meta-atom. Furthermore, the proposed method is also promising in high-performance antenna and radome design by arbitrarily and precisely modulating the complex field distribution over the whole aperture.

References

[1] L. Allen, M. W. Beijersbergen, R. Spreeuw, and J. Woerdman, "Orbital angular momentum of light and the transformation of Laguerre–Gaussian laser modes," *Phys. Rev. A, Gen. Phys.*, vol. 45, no. 11, pp. 8185–8189, Jun. 1992.

[2] M. Padgett and R. Bowman, "Tweezers with a twist," *Nature Photon.*, vol. 5, no. 6, pp. 343–348, 2011.

[3] J. E. Molloy and M. J. Padgett, "Lights, action: Optical tweezers," *Contemp. Phys.*, vol. 43, no. 4, pp. 241–258, Jul. 2002.

[4] J. Ng, Z. Lin, and C. T. Chan, "Theory of optical trapping by an optical vortex beam," *Phys. Rev. Lett.*, vol. 104, no. 10, Mar. 2010, Art. no. 103601.

[5] D. Wen et al., "Helicity multiplexed broadband metasurface holograms," *Nature Commun.*, vol. 6, p. 8241, Sep. 2015.

[6] Y. Yan et al., "High-capacity millimetre-wave communications with orbital angular momentum multiplexing," *Nature Commun.*, vol. 5, p. 4876, Sep. 2014.

[7] N. Bozinovic et al., "Terabit-scale orbital angular momentum mode division multiplexing in fibers," *Science*, vol. 340, no. 6140, pp. 1545–1548, Jun. 2013.

[8] J. Wang et al., "Terabit free-space data transmission employing orbital angular momentum multiplexing," *Nature Photon.*, vol. 6, no. 7, pp. 488–496, Jul. 2012.

[9] A. D. Wang et al., "Adaptive water-air-water data information transfer using orbital angular momentum," *Opt. Exp.*, vol. 26, no. 7, pp. 8669–8678, Apr. 2018.

[10] F. Tamburini, E. Mari, A. Sponselli, B. Thidé, A. Bianchini, and F. Romanato, "Encoding many channels on the same frequency through radio vorticity: First experimental test," *New J. Phys.*, vol. 14, no. 3, Mar. 2012, Art. no. 033001.

[11] L. Zhu and J. Wang, "Demonstration of obstruction-free data-carrying N-fold Bessel modes multicasting from a single Gaussian mode," *Opt. Lett.*, vol. 40, no. 23, pp. 5463–5466, Dec. 2015.

[12] P. Schemmel, G. Pisano, and B. Maffei, "Modular spiral phase plate design for orbital angular momentum generation at millimetre wavelengths," *Opt. Exp.*, vol. 22, no. 12, pp. 26–14712, Jun. 2014.

[13] M. W. Beijersbergen, R. P. C. Coerwinkel, M. Kristensen, and J. P. Woerdman, "Helical-wavefront laser beams produced with a spiral phaseplate," *Opt. Commun.*, vol. 112, pp. 321–327, Dec. 1994.

[14] N. R. Heckenberg, R. McDuff, C. P. Smith, and A. G. White, "Generation of optical phase singularities by computer-generated holograms," *Opt. Lett.*, vol. 17, no. 3, p. 221, Feb. 1992.

[15] M. Lin, Y. Gao, P. Liu, and J. Liu, "Theoretical analyses and design of circular array to generate orbital angular momentum," *IEEE Trans. Antennas Propag.*, vol. 65, no. 7, pp. 3510–3519, Jul. 2017.

[16] Q. Li et al., "Geometric phase based circular array for multimode vortex beam generation," *Annalen der Physik*, vol. 531, no. 12, Dec. 2019, Art. no. 1900367.

[17] B. Thide et al., "Utilization of photon orbital angular momentum in the low-frequency radio domain," *Phys. Rev. Lett.*, vol. 99, no. 8, Aug. 2007, Art. no. 087701.

[18] E. Karimi, S. A. Schulz, I. De Leon, H. Qassim, J. Upham, and R. W. Boyd, "Generating optical orbital angular momentum at visible wavelengths using a plasmonic metasurface," *Light, Sci. Appl.*, vol. 3, no. 5, pp. e167–e167, May 2014.

[19] N. Yu et al., "Light propagation with phase discontinuities: Generalized laws of reflection and refraction," *Science*, vol. 334, no. 6054, pp. 7–333, Oct. 2011.

[20] L. Zhang, S. Liu, L. Li, and T. J. Cui, "Spin-controlled multiple pencil beams and vortex beams with different polarizations generated by pancharatnam-berry coding metasurfaces," *ACS Appl. Mater. Interfaces*, vol. 9, pp. 36447–36455, Oct. 2017.

[21] Y. Bao, J. Ni, and C. Qiu, "A minimalist single-layer metasurface for arbitrary and full control of vector vortex beams," *Adv. Mater.*, vol. 32, no. 6, Feb. 2020, Art. no. 1905659.

[22] Z. Gong et al., "Broadband efficient vortex beam generation with metallic helix array," *Appl. Phys. Lett.*, vol. 113, no. 7, Aug. 2018, Art. no. 071104.

[23] C. Wu, Q. Li, Z. H. Zhang, S. Zhao, and H. Q. Li, "Control of phase, polarization, and amplitude based on geometric phase in a racemic helix array," *Photon. Res.*, vol. 9, no. 11, pp. 2265–2276, Nov. 2021.

[24] J. Ding, S. An, B. Zheng, and H. Zhang, "Multiwavelength metasurfaces based on single-layer dual-wavelength meta-atoms: Toward complete phase and amplitude modulations at two wavelengths," *Adv. Opt. Mater.*, vol. 5, no. 10, May 2017, Art. no. 1700079.

[25] Y. Yang, W. Wang, P. Moitra, I. I. Kravchenko, D. P. Briggs, and J. Valentine, "Dielectric meta-reflectarray for broadband linear polarization conversion and optical vortex generation," *Nano Lett.*, vol. 14, no. 3, pp. 1394–1399, Feb. 2014.

[26] R. Y. Wu et al., "Independent control of copolarized amplitude and phase responses via anisotropic metasurfaces," *Adv. Opt. Mater.*, vol. 8, no. 11, Jun. 2020, Art. no. 1902126.

[27] Y. Shuang, H. Zhao, W. Ji, T. J. Cui, and L. Li, "Programmable high-order OAM-carrying beams for direct-modulation wireless communications," *IEEE J. Emerg. Sel. Topics Circuits Syst.*, vol. 10, no. 1, pp. 29–37, Mar. 2020.

[28] Q. Feng, Y. Lin, M. Shan, Y. Mu, and L. Li, "Generation and measurement of a Bessel vortex beam carrying multiple orbital-angular-momentum modes through a reflective metasurface in the RF domain," *Phys. Rev. A, Gen. Phys. Appl.*, vol. 15, no. 6, Jun. 2021, Art. no. 064044.

[29] H. X. Xu et al., "Interference-assisted kaleidoscopic meta-plexer for arbitrary spin-wavefront manipulation," *Light, Sci. Appl.*, vol. 8, no. 1, p. 3, Jan. 2019.

[30] S. Li and J. Wang, "Adaptive power-controllable orbital angular momentum (OAM) multicasting," *Sci. Rep.*, vol. 5, no. 1, p. 9677, May 2015.

[31] H.-X. Xu et al., "Completely spin-decoupled dual-phase hybrid metasurfaces for arbitrary wavefront control," *ACS Photon.*, vol. 6, no. 1, pp. 211–220, Jan. 2019.

[32] Z.-L. Deng et al., "Full-color complex-amplitude vectorial holograms based on multi-freedom metasurfaces," *Adv. Funct. Mater.*, vol. 30, no. 21, Mar. 2020, Art. no. 1910610.

[33] H. X. Xu et al., "Chirality-assisted high-efficiency metasurfaces with independent control of phase, amplitude, and polarization," *Adv. Opt. Mater.*, vol. 7, no. 4, p. 10, Feb. 2019.

[34] L. Bao et al., "Multi-beam forming and controls by metasurface with phase and amplitude modulations," *IEEE Trans. Antennas Propag.*, vol. 67, no. 10, pp. 6680–6685, Oct. 2019.

[35] G. W. Ding et al., "Direct routing of intensity-editable multi-beams by dual geometric phase interference in metasurface," *Nanophotonics*, vol. 9, no. 9, pp. 2977–2987, Sep. 2020.

[36] H. Li, G. Wang, T. Cai, H. Hou, and W. Guo, "Wideband transparent beam-forming metadevice with amplitude- and phase-controlled metasurface," *Phys. Rev. A, Gen. Phys. Appl.*, vol. 11, no. 1, Jan. 2019, Art. no. 014043.

[37] C. Wu, Q. Li, S. Zhao, Z.-H. Zhang, S.-J. Wei, and H.-Q. Li, "Analytical full complex-amplitude control strategy for metasurface," *New J. Phys.*, vol. 23, no. 8, Aug. 2021, Art. no. 083023.
[38] *DongJun Technology, EastWave 6*. Accessed: Nov. 3, 2022. [Online]. Available: https://www.eastfdtd.com
[39] G. Molina-Terriza, J. P. Torres, and L. Torner, "Management of the angular momentum of light: Preparation of photons in multidimensional vector states of angular momentum," *Phys. Rev. Lett.*, vol. 88, no. 1, Jan. 2002, Art. no. 013601.
[40] D. Hakobyan, H. Magallanes, G. Seniutinas, S. Juodkazis, and E. Brasselet, "Tailoring orbital angular momentum of light in the visible domain with metallic metasurfaces," *Adv. Opt. Mater.*, vol. 4, no. 2, pp. 306–312, Feb. 2016.
[41] R. C. Devlin et al., "Spin-to-orbital angular momentum conversion in dielectric metasurfaces," *Opt. Exp.*, vol. 25, no. 1, pp. 377–393, Jan. 2017.
[42] K. Zhang et al., "Phase-engineered metalenses to generate converging and non-diffractive vortex beam carrying orbital angular momentum in microwave region," *Opt. Exp.*, vol. 26, no. 2, pp. 1351–1360, Jan. 2018.
[43] S. Jiang, C. Chen, H. Zhang, and W. Chen, "Achromatic electromagnetic metasurface for generating a vortex wave with orbital angular momentum (OAM)," *Opt. Exp.*, vol. 26, no. 5, pp. 6466–6477, Mar. 2018.
[44] M. Krenn et al., "Twisted light transmission over 143 km," *Proc. Nat. Acad. Sci. USA*, vol. 113, no. 48, pp. 13648–13653, Nov. 2016.

Quan Li (Member, IEEE) received the Ph.D. degree in condensed matter physics from Tongji University, Shanghai, China, in 2019.

He is currently holding a post-doctoral position at Tongji University. His research interests include structured light manipulation, vortex-mode communication application, and metasurface design for antennas and imaging applications.

Chao Wu (Member, IEEE) received the Ph.D. degree in condensed matter physics from Tongji University, Shanghai, China, in 2012.

He is currently an Associate Professor with Tongji University. His research interests include the chiral symmetry in metamaterial, multidimensional manipulation of the electromagnetic field, and the active metasurface and its application in antenna designs.

Zhihui Zhang is currently pursuing the Ph.D. degree with the Shanghai Key Laboratory of Special Artificial Microstructure Materials and Technology, School of Physics Science and Engineering, Tongji University, Shanghai, China.

His research interests include metasurface and surface wave.

Song Zhao is currently pursuing the Ph.D. degree with the Shanghai Key Laboratory of Special Artificial Microstructure Materials and Technology, School of Physics Science and Engineering, Tongji University, Shanghai, China.

His research interests include polarization manipulation in metasurface and its application in vortex beam generation.

Bin Zhong is currently a Senior Engineer with the Institute of Dongguan-Tongji University, Guangdong, China.

His research interests include structural–functional ceramic material and its application in complex electromagnetic field manipulation.

Song Li is currently a Senior Engineer with the State Key Laboratory of Advanced Fiber Composite, Beijing, China.

His research interests include medium materials, composites, and ablative materials.

Hongqiang Li received the Ph.D. degree in optics from the Institute of Physics, Chinese Academy of Science, Beijing, China, in 1997.

He has been a Professor with Tongji University, Shanghai, China, since 2005. His research interests include the fundamental physics in subwavelength systems, the optical properties in metamaterial, and the advanced applications.

Lijun Jin received the B.S., M.S., and Ph.D. degrees in electrical engineering from Xi'an Jiaotong University (XJTU), Xi'an, China, in 1987, 1997, and 2000, respectively.

He held a post-doctoral position at Tsinghua University, Beijing, China, in 2000. From 1989 to 1994, he was at Xi'an High-Voltage Apparatus Research Institute Company Ltd., Xi'an. He is currently a Professor with the Department of Electrical Engineering, Tongji University, Shanghai, China. His research fields involve simulation and analysis for electromagnetic field, research and development of high-voltage electrical equipment, measurement and fault diagnosis on line for electrical equipment, and high-voltage technology.